Annual Report May 2004

Novel Image Analysis to Link Sub-Nuclear Distribution of Proteins with Cell Phenotype in Mammary Cancer

Investigators: David Knowles (Collaborating laboratories: Sudar, Lelièvre, Bissell)

ABSTRACT:

The goal of this project is to develop novel optical imaging / image analysis techniques that will allow automated, quantitative screening to distinguish malignant, pre-malignant, and non-malignant mammary tissue. Our hypothesis is that cellular and tissue phenotype is reflected by the organization of components within the nucleus. By quantifying the spatial distribution of these proteins in this relevant culture model system, the work will provide understanding of how such distributions correspond with the phenotype of the cells. The work focuses on the distribution structural nuclear proteins in a progression series of cultured HMT-3522 human mammary epithelial cells (HMECs) that mimic early stages of cancer development. To quantify these distributions we have extended our image analysis capability to allow the relative density of NuMA foci to be measured within an individual nucleus and thus on a per nucleus basis. Automation of the these methods have enabled us to analyze thousands of nuclei. This technique has revealed striking reorganization of NuMA during acinar morphogenesis, while no such reorganization occurred during tumor formation. The discrimination between proliferating non-malignant cells and proliferating malignant cells based on the automated analysis of the distribution of a nuclear protein has not previously been achieved.

INTRODUCTION:

The goal of this project is to develop novel optical imaging / image analysis techniques that will allow automated, quantitative screening to distinguish malignant, pre-malignant, and non-malignant mammary tissue. Our hypothesis is that cellular and tissue phenotype is reflected by the organization of components within the nucleus. By quantifying the spatial distribution of these proteins in this relevant culture model system, the work will provide understanding of how such distributions correspond with the phenotype of the cells.

BODY:

The work focuses on the distribution structural nuclear proteins in a progression series of cultured HMT-3522 human mammary epithelial cells (HMECs) that mimic early stages of cancer development. Non-malignant S1 HMT-3522 cells recapitulate differentiation into phenotypically normal breast glandular structures in 10 day of three-dimensional (3D) culture. 3D culture is preformed by placing cells in contact with an exogenous extracellular matrix enriched in basement membrane components (Matrigel), and supplying cells with essential growth factors and hormones. Glandular structure formation encompasses cell proliferation (until day 6), growth-arrest and deposition of a continuous endogenous basement membrane around the glandular structure. Malignant T4-2 HMT-3522 cells mimic tumor growth, with the formation of disorganized

multicellular structures in which cells keep proliferating, when cultured in the same conditions. Nuclear mitotic apparatus, NuMA, protein has been previously found to undergo remarkable changes in its nuclear organization during glandular structure formation (Lelièvre et al., 1998). During the proliferating stage the distribution patterns of NuMA appear homogenous throughout the cell nucleus and was seem similar to what is observed in tumor cells. Whereas, upon differentiation, NuMA is reorganized into foci within the cell nucleus and ring-like patterns at its periphery. Culturing of the cells and fluorescence labeling of the NuMA protein was be carried out, under subcontract, at the Lelièvre laboratory at Purdue University. Image collection, the development of novel image analysis techniques and the image analysis has be performed at our facility at LBNL.

Key outcomes of the first year of work (Months 1 - 12) were the acquisition of images of NuMA organization in cells cultured between 4 and 12 days and the development of a local bright feature (LBF) analysis method. Previously we had only studies proliferating cells at 4 to 5 days of culture, but after 10 days of culture, nonmalignant cells have differentiated into acini and malignant cells have proliferated into large unorganized clusters. Analyzing images from these cultures has strengthened our initial hypothesis about the reorganization of NuMA in nonmalignant cells and this has been key in the further development of our image analysis techniques. The LBF analysis method we developed allows bright foci within a nucleus to be isolated from the diffuse NuMA staining.

In the second year of work (Months 13 - 24) we have maintained our primary focus on quantifying the distribution of NuMA and extended our image analysis capability to allow the distribution of NuMA foci to be measured within an individual nucleus and thus on a per nucleus basis. Briefly, this has been achieved by several key developments. 1) Our nuclear segmentation ability has been extended to allow automated segmentation of individual nuclei from a cluster of cells. 2) Our local bright feature (LBF) analysis has been modified to allow both local bright and local dark features within a nucleus to be isolated for further analysis. 3) Image analysis techniques were developed to allow each nuclear volume to be subdivided into a set of concentric terraces. These refinements have allowed us to calculate the relative density of NuMA foci in each nucleus, on a per terrace basis and evaluated as an effective radial distribution from the perimeter of the nucleus to its center.

These methods have allowed us to representing the distribution of NuMA bright features associated with different mammary phenotypes as a simple graph, hence enabling an easy interpretation of the spatial distribution of the protein. The performance of the LBF analysis was greatly enhanced by the development of an automated segmentation of the nuclear volume that enabled us to analyze thousands of nuclei in a short period of time. Using this novel image analysis technique we measured the striking reorganization of NuMA during acinar morphogenesis, while no such reorganization occurred during tumor formation. Most importantly, the LBF analysis permitted a clear discrimination between proliferating non-malignant cells and proliferating malignant cells, which was not achieved so far using other evaluation methods.

Significant progress has been made in the last year.

Methods:

1) Automated Segmentation of Individual Nuclei from 3D Images

One of the key developments of the last year is a segmentation algorithm which automatically determines the position and extent of individual nuclei within DAPI-stained images. The automatic nuclear segmentation method was developed, based on a local threshold, a template matching and region growing techniques. An adaptive threshold algorithm was applied to the DAPI-stained image to separate image pixel within nuclei from those outside nuclei and produced a binary mask of all the nuclei. The technique uses a difference-of-Gaussians filter (Marr 1982), followed by a closing filter and then remaining holes within the mask were filled with a flood-fill algorithm. This local threshold algorithm accurately separates nuclei from their background but does not isolate neighboring nuclei when they are tightly clustered. To separate touching nuclei, specific morphological information was used about the objects. While the nuclei in epithelial cells and in our HMT-3522 cell culture system often have irregular shapes, they are of simple geometry which encompasses a single spherical core. Individual nuclei were thus located using standard template matching techniques (Haralick & Shapiro 1992) to locate the central nuclear core. Once found, the central core was dilated into the rest of the nucleus using region-growing techniques. To do this, a template, with dimensions that approximate the average spherical core of nuclei, was convolved with the binary nuclear mask. This convolution produced a map that indicated the percentage of the template that fit within the binary mask at each point in the image. Next, the template was stamped into the binary mask at locations where there were corresponding local maxima in the map that exceeded 70%. The templates were stamped at the center-of-mass of the local maximum, in an order ranked by their percentage, starting from the highest. A template was not stamped if it overlapped a previously stamped template by more than 70%, or if the local maximum was at the boundary of the binary mask. Objects with less than 70% match were discarded. Similarly, if local maxima occurred at the boundary of the segmentation mask due to proximity of neighboring nuclei, they were not taken into account. Once all the nuclear cores were located, each template was dilated in a semi-intelligent fashion into the binary mask. Briefly, template dilation was done independently in the positive and negative X, Y, and Z directions. Dilation along any particular direction was halted when 60% of the dilating template boundary reached the boundary of the binary mask. This prevented a dilating template in one nucleus from squeezing through narrow regions in the binary mask that connected two adjacent nuclei. In addition, dilation was stopped in all directions if the volume of the dilated template exceeded nine times its original volume. This phenomenon occurred if nuclei were piled up on each other and the segmentation mask failed to separate them adequately. When encountered, this phenomenon was reported as a segmentation error and the segmentation attempt was canceled.

2) Distribution Analysis of NuMA

Several key developments this last year have enable quantification of NuMA distribution within a nucleus. Refinements to our LBF analysis allow both local bright and local dark features to be extracted from a nucleus. In the initial version of this analysis only local bright features were extracted but, as discussed below, being able to extract local dark features has allowed us to account for the absence of NuMA with nucleoli. Compartmentalizing individually segmented nuclei into a set of concentric terraces has allowed the quantification of the radial distribution of NuMA within individual nuclei.

Following immunostaining, image acquisition and segmentation, NuMA foci were isolated by a technique referred to as the local bright feature (LBF) analysis. Pixel brightness in the raw NuMA images was normalized by the local average brightness using an extension of the difference-of-Gaussians technique (Marr 1982). The raw NuMA image was first multiplied by the binarized segmentation mask used to isolate individual nuclei. Then, image brightness within each nucleus was rescaled by dividing the brightness at each point by the local average brightness about that point. The local average brightness was calculated over a region with a dimension half that of the dimension of the nuclear core. This was very important. The region had to be larger than any bright or dark features to be resolved, but smaller than the nucleus itself. This allowed bright foci and dark regions within the nucleus to be resolved and low frequency brightness variations due to the geometry of the nucleus and the axial resolution of the microscope to be removed. Bright image features have values above unity in the resulting LBF images, while dark image features have values below unity. To enable the radial distribution of the local bright features to be calculated, a distance transform (Haralick & Shapiro 1992) was applied to the nuclear segmentation mask. The transform calculates the distance of each point within a nucleus from its nearest boundary and in doing so, divides each nucleus into a set of concentric equal thickness terraces. The LBF image was then used in conjunction with the nuclear segmentation mask and its distance transform to compute the density of local bright features in each terrace of each nucleus. The density was calculated for each terrace as the number of pixels in local bright features divided by the total number of pixels. The density per terrace was then normalized so that the average density of foci is unity for each nucleus. The distances defined by the distance transform were also normalized so that the distance at the nuclear perimeter was 0.1 and the distance at the center of the nucleus was 1.0. Finally, the normalized density of foci was plotted against normalized distance from the perimeter of the nucleus to its center.

Results:

Radial distribution analysis in acinar cells reveals a peak of NuMA foci density centered on a shell located midway between the periphery and the center of the nucleus.

The organization of NuMA in the nucleus displays intricate, three-dimensional, spatial distributions that vary with changes in cell and tissue phenotypes. Visual analysis of immuno-stained NuMA reveals that NuMA aggregates into bright foci, but it is also present, with less brightness, diffusely throughout the nucleus (Lelievre et al., 1998).

Specifically, the density of foci and their distribution within the nucleus appeared dependent on the phenotype. To quantify the distribution of NuMA, we have constructed a method that calculates the radial distribution of the density of NuMA foci within each nucleus. S1 cells were cultured in 3-D to induce acinar morphogenesis where NuMA foci are most abundant. Acini were immunostained for NuMA (figure 1B) and counterstained with DAPI (figure 1A). A segmentation mask was created from the DAPI image to isolate the position and extent of individual nuclei (figure 1C). Then, bright features of NuMA staining were isolated from the diffuse NuMA staining using the LBF analysis. Results of this analysis created a rescaled image, referred to as LBF image, in which the pixel values above 1 represent bright features and pixel values below 1 represent dark features. As a visual demonstration of how this process works, local bright features isolated by the LBF method have been overlayed with the segmentation mask to show the position of these features in relation to the nuclear boundary (figure 1 D). This method permitted a clear visualization of the localized accumulation of NuMA throughout the nucleus. Results indicated that the density of NuMA bright features was low at the periphery of the nucleus and varied with depth into the nucleus. We used this observation to quantify NuMA distribution as a function of the depth into the nucleus. A distance transform was applied to the segmentation mask to subdivide each nuclear volume into a set of concentric terraces of equal thickness, starting at the nuclear perimeter (figure 1E).

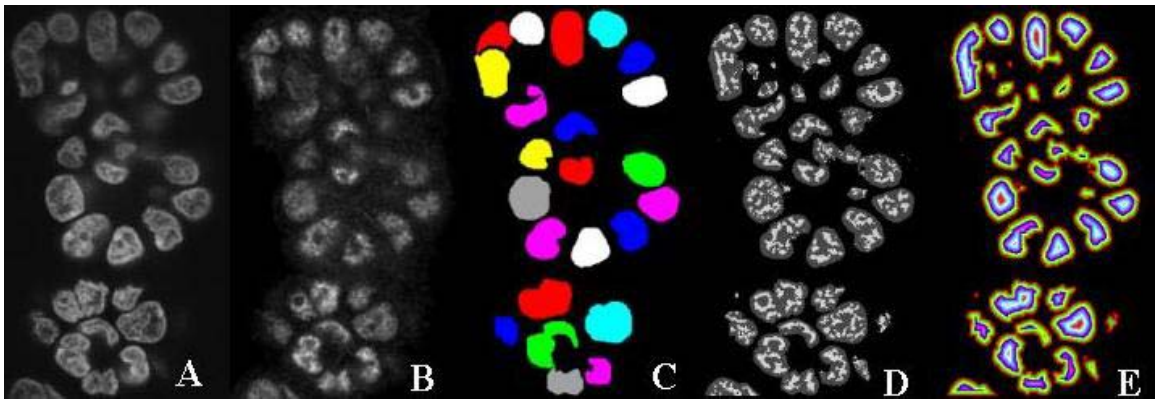

Figure 1. Distribution density of NuMA foci in acinar cells.
HMT-3522 S1 HMECs were cultured in 3-D to induce acinar morphogenesis. Each panel corresponds to the application of the different steps of distribution analysis starting from the same original image **A.** Fluorescence micrograph of DAPI-stained nuclei from a single optical section containing three acini. **B.** Fluorescence micrograph of Texas-red immunolabeled NuMA from the optical section corresponding to the DAPI image shown in A. **C.** Segmentation mask derived from the DAPI-stained image showing a single slice of individually numerated nuclei. **D.** Composite view of the local bright features (light gray) extracted by the LBF analysis overlayed with the segmentation mask (dark gray). **E.** Concentric terraces resulting from the application of the distance transform on the segmentation mask.

The distance transformed-segmentation mask was combined with the LBF image to calculate the variation of the relative density of NuMA bright features as a function of the relative distance from the perimeter of the nucleus into its center. To demonstrate the consistency of this method, the distribution results were plotted for 77 nuclei analyzed within a single image (figure 2). As the visual representation indicated (figure 1C), the density of NuMA bright features was below the average density at the perimeter of the nuclei and monotonically increased above the average density to reach a peak midway between the perimeter and the center of the nucleus.

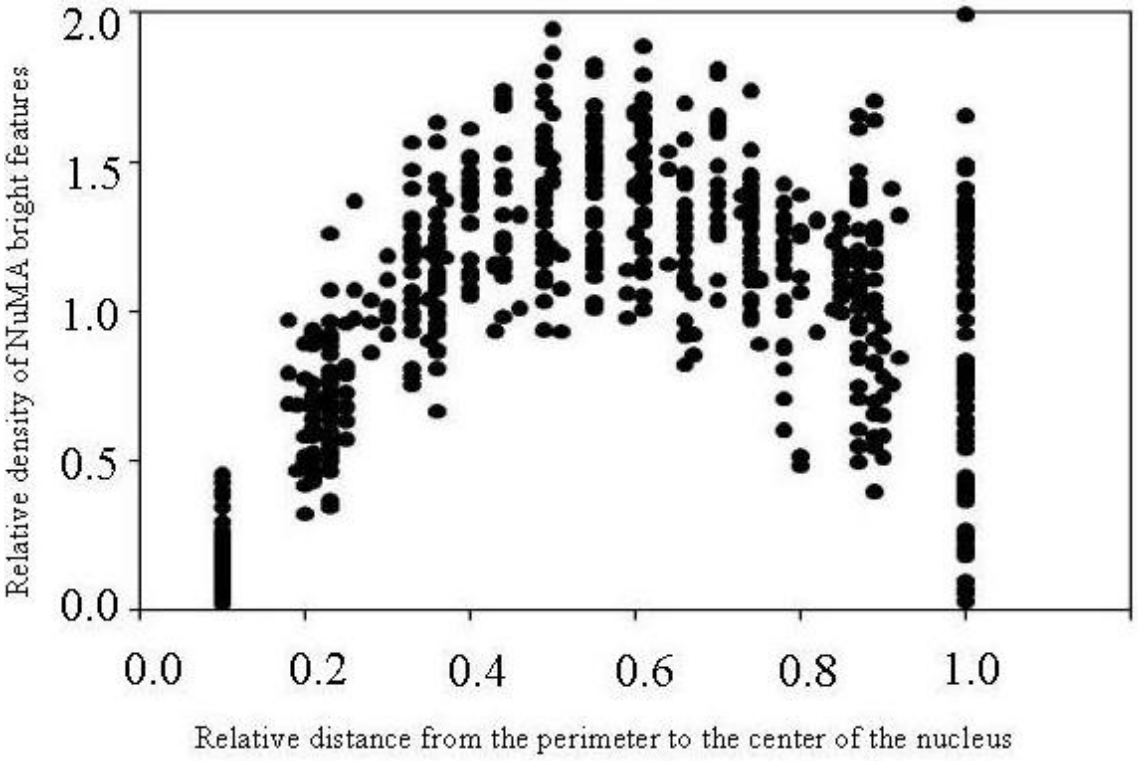

Figure 2. Relative density of local bright features of NuMA in 77 nuclei from a single image of three acini.
HMT-3522 S1 HMECs were cultured in 3-D to induce acinar morphogenesis. Multi-overlay plot of the relative density of NuMA bright features extracted by LBF analysis (ordinate) vs. relative distance from the perimeter to the center of each nucleus (abscissa).

The repartition and the density of NuMA bright features changes as a function of acinar morphogenesis.
Previous analysis of NuMA immunostaining during the proliferation stage (day 3 of 3-D culture) and upon acinar differentiation (day 10 of 3-D culture) suggested that there was an increase in the foci-like feature of NuMA upon completion of acinar morphogenesis (Lelievre et al., 1998). This analysis was based on visual estimation and the manual measurement of the size of NuMA foci on images of NuMA staining. Thus, this

painstaking and non-powerful quantitative analysis only enabled us to get a gross comparison of the redistribution of NuMA during morphogenesis. To assess the efficiency of the LBF analysis in measuring reproducibly the changes in NuMA distribution along the morphogenesis process, we cultured S1 HMECs in 3-D for 3, 5, 10 and 12 days and applied the LBF analysis to NuMA immunostaining as described above. The LBF analysis revealed that both the density and the distribution of bright features of NuMA immunostaining were modified during acinar morphogenesis. The density of bright features above the average density covered an increasing number of terraces from day 3 to 10 of 3-D culture (figure 3), thus confirming our initial observation that acinar morphogenesis is accompanied by an increase in NuMA foci (Lelievre et al., 1998). Most interestingly, the LBF analysis revealed that the densest population of bright features of NuMA progressively redistributed towards the interior of the nucleus, as shown by the displacement of the peak of the curve (figure 3). Upon acinar differentiation, there was also a decrease in density of bright features of NuMA in the peripheral terraces, as seen for day 10 and 12 of 3-D culture. Similar density distributions were obtained with two different antibodies directed against NuMA. Images recorded at high magnification showed that in acinar cells NuMA staining was usually absent from most of the periphery of the nucleus.

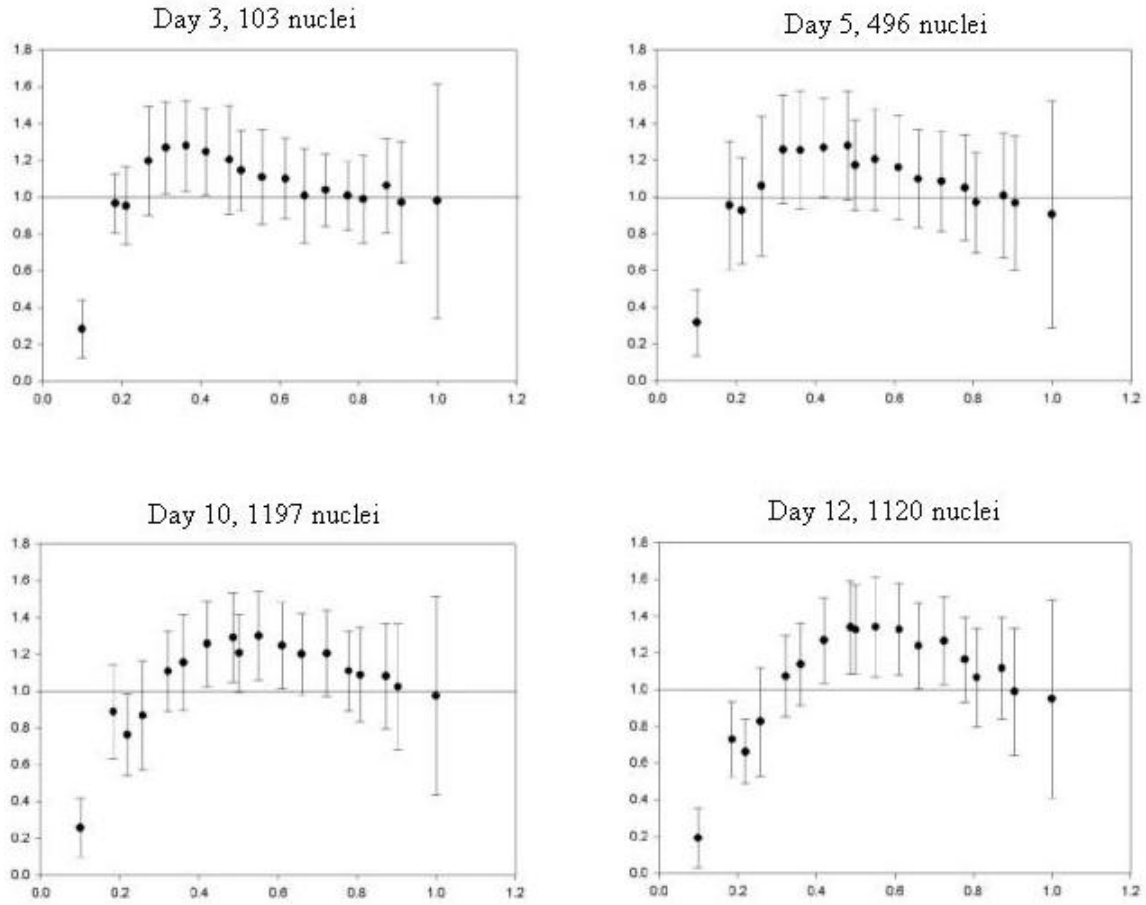

Figure 3. Average relative density of local bright features of NuMA during acinar

morphogenesis.
S1 cells were cultured in 3-D for 3, 5, 10 and 12 days. Plots represent the relative density of NuMA bright features extracted by LBF analysis (ordinate) vs. relative distance from the perimeter to the center of a population of nuclei for each time point (abscissa). The number of nuclei for each time point is indicated above each corresponding graph. Bars represent the standard deviation.

The distribution of NuMA bright features in malignant T4-2 cells differs from both proliferating and differentiated non-neoplastic S1 cells.

In non-differentiated proliferating S1 cells NuMA distribution is more diffuse than in growth arrested (day 5 of 3-D culture) and polarized (day 10 of 3-D culture) acinar cells. We asked whether the diffuse distribution of NuMA was a characteristic of a cell population actively proliferating, regardless of the origin, non-neoplastic or malignant, of the cells. As expected, immunostaining of malignant T4-2 cells for NuMA after 10 days of 3-D culture showed that this protein was mostly diffusely distributed and that overall this distribution did not seem visually different from that observed in proliferating non-neoplastic S1 cells. Similarly to our data with acinar cells (Lelievre et al., 1998), the distribution of NuMA in tumor-like nodules obtained in 3-D culture was not visually different from the distribution of NuMA in biopsy samples of invasive carcinoma (not shown). To quantitatively assess our visual observation, we applied the LBF analysis to 3-D cultures of T4-2 cells at days 4, 5, 10 and 11. As described earlier, increasing length of culture resulted in increasing sizes of disorganized tumor-like nodules. In contrast to non-neoplastic cells, the LBF analysis showed a fairly flat distribution of NuMA bright features in malignant cells, regardless of the number of days in 3-D culture and hence of the size of the tumor nodules (figure 4). Thus, in agreement with the fact that there were no significant alterations in the phenotype of tumor nodules, expect for their size, during 11 days of 3D culture, there was no apparent change in the density of NuMA bright features throughout the nuclei of tumor cells during this culture period.

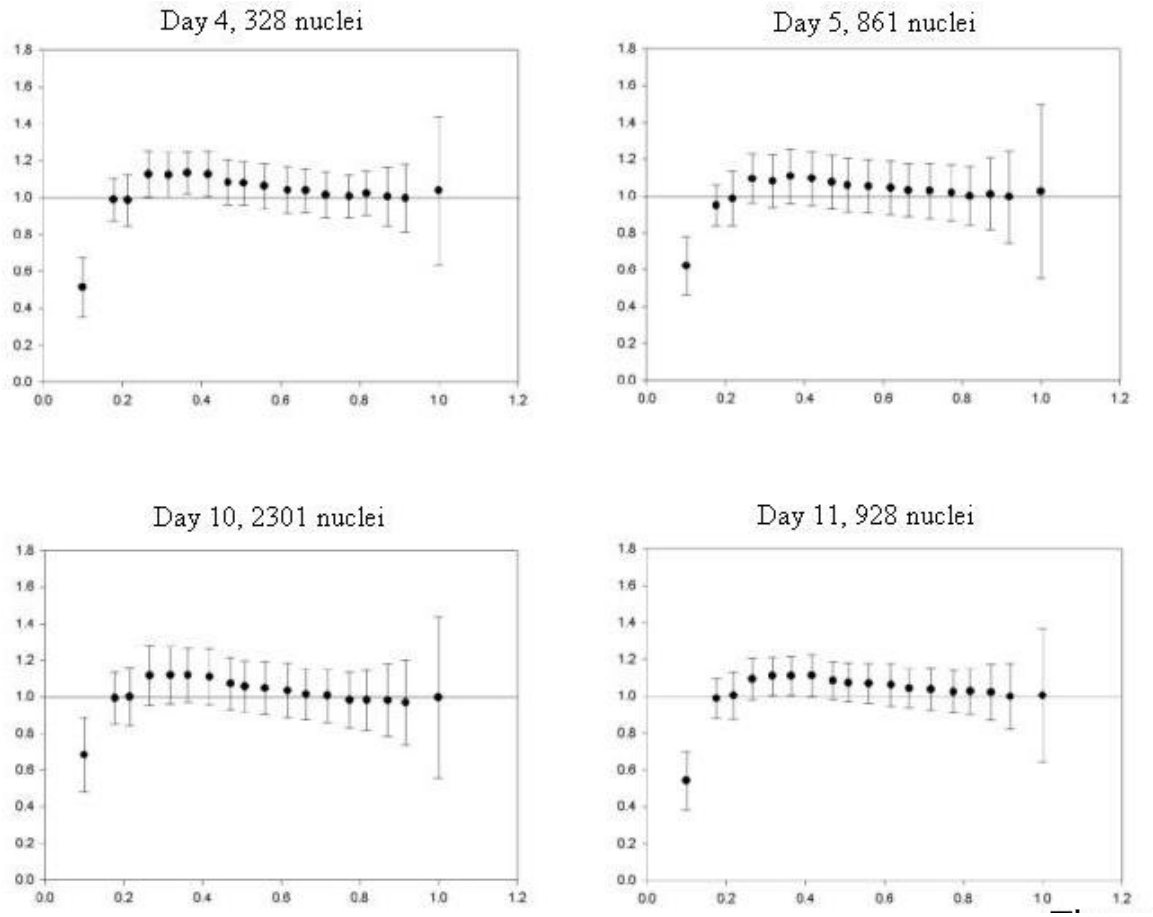

Figure 4. Differences in the relative density of NuMA bright features between non-neoplastic and malignant cells.
T4-2 cells were cultured in 3-D for 4, 5, 10 and 11 days. Plots represent the relative density of NuMA bright features extracted by LBF analysis (ordinate) vs. relative distance from the perimeter to the center of a population of nuclei for each time point (abscissa). The number of nuclei for each time point is indicated above each corresponding graph. Bars represent the standard deviation.

The distribution curves of the density of bright features of NuMA did not clearly show a peak at any of the time points, suggesting that there was a difference in NuMA distribution not only between malignant T4-2 cells and acinar S1 cells, but also between malignant T4-2 cells and proliferating S1 cells. To better visualize the differences in the distribution of the bright features of NuMA for the different phenotypes and time points described above, we plotted the cumulative density of NuMA bright foci as a function of the volumetric terraces used to apply the distance transform. The cumulative plots unambiguously showed that the distribution of the bright foci of NuMA was consistently similar for the different culture time points of the malignant T4-2 cells and that such a distribution was remarkably different from any of the stages, including proliferation, of acinar morphogenesis (figure 5).

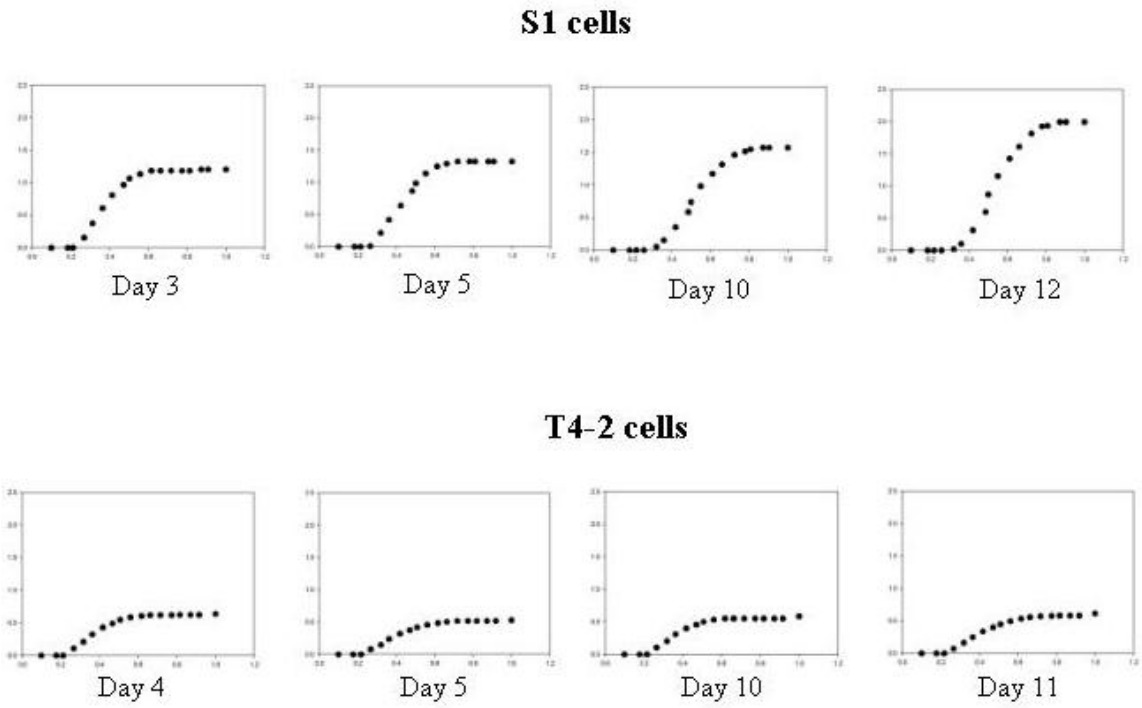

Figure 5. Differences in the cumulative density of NuMA bright features between non-neoplastic and malignant cells.
Cumulative plots of the relative density of NuMA bright features (ordinate) at different time points of 3-D culture of S1 and T4-2 cells vs. relative distance from the perimeter to the center of the nucleus (abscissa). Cumulative plots were prepared from the relative density data shown in figures 3 and 5A.

KEY RESEARCH ACCOMPLISHMENTS:

* A segmentation algorithm was developed to automatically define the position and extent of nuclei in 3D images.
* The local bright feature analysis was refined to extract local dark as well as local bright features from within images nuclei fluorescently stained for specific nuclear proteins.
* Compartmentalization of individual nuclei into a set of concentric terraces allows the quantification of the radial distribution of specific labeled proteins in individual nuclei.
* Application of these automated imaging techniques to reveal sticking differences in the organization of NuMA between proliferating non-malignant cells and proliferating malignant cells.

REPORTABLE OUTCOMES:

Drs Lelievre and Knowles have been awarded two grants in the last year based on this work.

Drs Lelievre and Knowles have been granted an exploratory 2 year award from Friends You Can Count On, FYCCO, a nonprofit organization dedicated to promoting awareness and education about breast cancer and to raising funds for research into earlier detection of breast cancer. http://www.earlier.org/index.html

Drs Lelievre and Knowles have notified that our DOD concept award, to find malignant cells within a population of benign cells, has been recommended for funding.

Drs Knowles and Lelievre have a manuscript in preparation.

CONCLUSIONS:

The automated image analysis methods established in the last year have allowed us to simply represent the distribution of NuMA bright features associated with different mammary phenotypes as a simple graph, which enables easy interpretation of the spatial distribution of the protein. These novel techniques have revealed striking reorganization of NuMA during acinar morphogenesis, while no such reorganization occurred during tumor formation. They have permitted a clear discrimination between proliferating non-malignant cells and proliferating malignant cells, which was not achieved so far using other evaluation methods. These results about the distribution of NuMA within our model cell culture system set the stage for evaluating the organization of a range of other structural nuclear proteins, particularly in normal and malignant human tissue.

REFERENCES:

Lelievre SA, Weaver VM, Nickerson JA, Larabell CA, Bhaumik A, Petersen OW, Bissell MJ. 1998
Tissue phenotype depends on reciprocal interactions between the extracellular matrix and the structural organization of the nucleus. Proc Natl Acad Sci U S A. 95:14711-6

Haralick R.M., Shapiro L.G., Computer and Robotic Vision Vol1 1992
Addison-Wesley ISBN 0-201-10877-1

Marr D., Vision 1982
W.H. Freeman & Co. ISBN 0-7167-1567-8

APPENDICES:
